Calibration and sensitivity of resonant-mass gravitational wave detectors

A. Morse, W. O. Hamilton, W. W. Johnson, E. Mauceli,* and M. P. McHugh
Department of Physics and Astronomy, Louisiana State University, Baton Rouge, Louisiana 70803-4001
(Received 31 August 1998; published 22 February 1999)

Every gravitational wave detector needs reliable methods for quantitative tests of its performance. We have tested the ALLEGRO gravitational wave antenna with a capacitive transducer which can apply a force to the antenna. A model that incorporates mistuning of the two normal modes of the antenna is needed to properly understand its operation and to explain previous discrepancies in calibration responses. We write the transfer functions for driving point response, signal response, and noise response in terms of a parameter θ which includes all of the mistuning. Using the ''reciprocity method,'' we determine θ and the force-voltage constant of the force generator. Using diagnostic criteria developed from a full multimode description, we are able to identify the location of an additional parasitic resonance and determine its quantitative effect on the results. Experimental results are presented. [S0556-2821(99)02606-5]

PACS number(s): 04.80.Nn, 95.55.Ym

I. INTRODUCTION

Resonant-mass gravitational wave detectors are currently in operation at several sites around the world. Research groups at the University of Rome and the INFN operate the EXPLORER, NAUTILIS, and AURIGA detectors [1,2], the research group at the University of Western Australia (UWA) operates the NIOBE detector [3], and our research group at Louisiana State University (LSU) operates the ALLEGRO detector [4]. These detectors are designed to look for the ''bursts'' of gravitational radiation that may be emitted during the gravitational collapse of a star or the final seconds of a binary coalescence [5]. Such events will be short-lived, infrequent, and of very small amplitude. If any claim of detection for such events is to be credible, there will need to be considerable proof that the detectors are working properly.

A resonant detector system is a linear, narrowband sensor of gravity waves. Like any real sensor, resonant antennas have intrinsic noise sources. There are two distinct parts to determination of sensitivity. First, there is a precise determination of how detector output is related to a gravitational signal. Second, there is a measurement of the detector's stationary noise. The stationary noise determines the smallest signal that can be detected and the nominal uncertainty of a measurement.

The first models of resonant mass gravitational wave detectors calculated sensitivity by treating the system as a single harmonic oscillator driven by noise [6,7]. The extension of this model to multimode systems demonstrated that detector sensitivity could be improved by increasing the number of modes, first to 2 [8,9], then to 3 or more [10–12]. These analyses concentrate on describing how fundamental noise sources appear at the output after being modified by the oscillator's transfer function. Good agreement was observed between the results from the numerical two-mode model and the output observed from two-mode systems [13]. The comparison between model and experiment required some theoretical estimation of the detector's physical parameters.

Boughn *et al.* showed how the response of the system to a signal can be determined without relying on any theoretical estimates of the system's physical parameters [14]. Their procedure measures the signal ''gain'' of each mode of a multimode detector. The model of Boughn *et al.* consists of two basic elements, a model of the antenna and transducer system used as the sensor of gravity waves and a model of the force generator used to apply calibration signals.

Boughn *et al.* assumed that the bare antenna and bare transducer had the same resonant frequency and treated the two mode system as two independent antennas. In their results, they reported that the two modes of the system respond differently to equal sized calibration signals, but offered no explanation of this fact. The two modes of ALLEGRO also respond differently to equal sized calibration signals. This result cannot be explained if the assumption perfect tuning between the modes is kept. The modeling of Boughn *et al.* leaves open the question of whether the different observed responses result from an experimental uncertainty, something unique to the systems where they have been measured, or a property of all multimode systems. By dispensing with the assumption of a perfectly tuned antenna-transducer system, we show that the observed differences are a property of all multimode systems.

Section III of this paper presents a description of a resonant bar gravitational wave antenna completely expressed in terms of measurable parameters. This description takes the form of a set of transfer functions describing the antenna system's response to different signal and noise sources. In Sec. IV, we show that our model of the antenna and transducer combined with the procedure developed by Boughn *et al.* determines the parameters of transfer functions for signal, noise, and calibration response without relying on theoretical estimates of the detector's physical parameters. This result also makes clear how mechanical mistuning between the antenna and transducer appears in the calibration procedure.

In Sec. V, we study the transfer function which describes

*Present address: INFN Laboratori Nazionali di Frascati, Via Enrico Fermi 40, I-00044 Frascati (Roma), Italy.

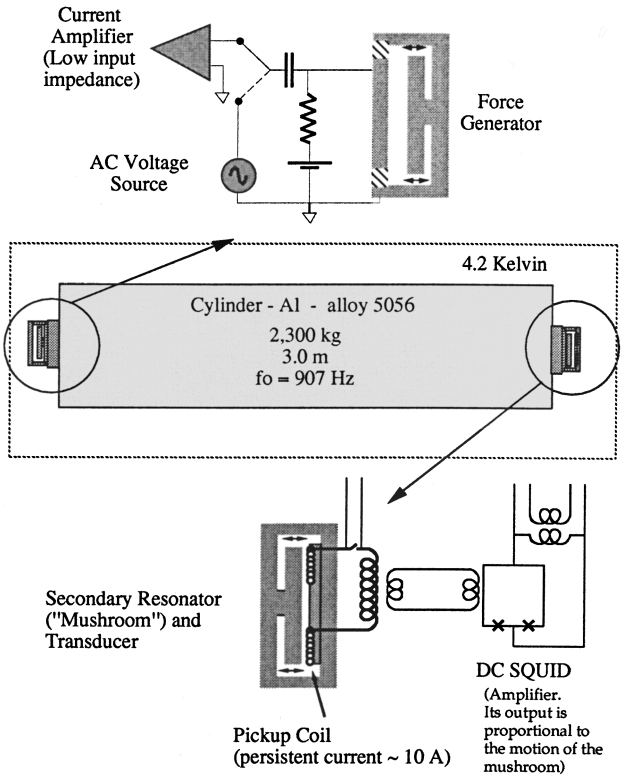

FIG. 1. A physical schematic of the ALLEGRO detector, including the primary inductive transducer and capacitive force generator.

the propagation of signals through the system. Historically, the relation between incident burst and detected output has been described in terms of the energy deposited in the antenna modes [14]. With imperfect tuning, this description can be misleading, because the burst does not deposit equal amounts of energy in both modes. In Sec. VI, we study the transfer function related to the antenna's dominant source of noise, and determine how it is affected by mechanical mistuning.

In Sec. VII, we compare the predictions of the model to the output of ALLEGRO. In the course of this examination, we found that a previously unexplained resonant mode in the detector response threatened substantial uncertainties in our understanding of the detector's sensitivity. An additional measurement was undertaken and a more comprehensive model was developed. From these, we have been able to determine the nature of this resonance and to show that overall detector response to a signal is quite close to the expected value. These results demonstrate the importance of carefully studying the relationships between modes in order to verify that the detector works as designed.

II. ALLEGRO DETECTOR

The ALLEGRO detector is a resonant-mass gravitational wave detector designed and constructed for the purpose of directly observing gravitational radiation. The ALLEGRO system, shown schematically in Fig. 1, is similar to the other resonant-mass detectors currently in operation. The largest component of ALLEGRO is a 3.0 m long solid circular cylinder of mass 2296 kg composed of aluminum alloy 5056. It is cooled to 4.2 K to reduce thermal noise and to take advantage of the high mechanical quality factors and superconducting properties of materials at low temperature.

The effect of the wave field on the antenna can be derived from the general relativistic equation of geodesic deviation [15]. In a system where the coordinates ξ_i measure distances in the laboratory frame, a gravity wave produces an effective force on a mass element dm of an isotropic body given by

$$df_i^G = dm \sum_j \frac{1}{2} \ddot{h}_{ij}(t) \xi_j , \tag{1}$$

where $h_{ij}(t)$ is the metric deviation in the transverse traceless gauge describing the wave field. df_i^G has the linear variation with position of a ''tidal'' force. Physically, Eq. (1) implies that a gravity wave creates a stress on the bar by accelerating different parts of the bar at different rates. The magnitude of the stress is proportional to the length of the bar.

Resonant bars are based on the principle that an incident gravity wave excites vibrational motion in the antenna. From the theory of elasticity, the vibration of a mass element of the antenna due to the net force applied by its neighbors can be described in terms of eigenfunctions determined by the shape of the body [16]. The eigenmode amplitudes, $x_m(t)$, solve a driven harmonic oscillator equation, where $x_m(t)$ is a ''collective coordinate'' representing coherent motion of the entire bar with spatial variation given by its eigenfunction [17].

We monitor the vibration of the lowest longitudinal mechanical resonance of the antenna and infer the sizes of incident excitations by measuring changes in the vibrational amplitude. If we consider the bar alone (without resonator), and only make measurements near the 1st mode frequency, the elastic motion of the bar can be described with a harmonic oscillator equation for its first mode. Non-elastic forces, including gravitational forces, are described as external forces applied to the oscillator. Separating the non-elastic forces into gravitational and non-gravitational components,

$$x_1(t) + \omega_1^2 x_1(t) = \frac{1}{m_1}[F_G(t) + F_{NG}(t)], \tag{2}$$

where F_G is the net force resulting from integrating the force density df_1^G over the elastic body, F_{NG} is the net force from non-gravitational sources acting on the antenna, and m_1 is the effective mass of the antenna. m_1 is equal to one-half of the bar's physical mass, resulting from equating the collective coordinate $x_1(t)$ to the displacement of the end face of the antenna [17].

A smaller mechanical resonator, also called the transducer, is attached to one face of the antenna. Together, the antenna and resonator form a system of two damped, coupled oscillators. The damping is small due to the use of extremely low-loss materials [18]. Since searches for burst sources involve monitoring the system for changes created by impulses whose duration is much shorter than the damp-

ing time, it is a good approximation to ignore the damping. A superconducting coil and superconducting quantum interference device (SQUID) amplifier are used to measure the relative motion between the resonator and the end of the bar [19]. This readout system produces a voltage directly proportional to the differential displacement between the antenna face and the resonator's pick-up coil.

A capacitive transducer, or force generator, is mounted at the other end of the bar. A voltage applied to the force generator applies a force on the end of the bar, the size of which depends on the geometry of the device. The force generator is a reciprocal device, meaning it can also be used to detect motion. In detection mode, we measure the voltages and currents that result when mechanical forces are applied to the capacitor plates. By measuring the motion that has been produced immediately after the antenna is excited with the force generator, the generator constant, defined as the ratio of voltage applied at the electrical terminals to force applied at the antenna face, is determined. Once the generator constant is known, test signals of known strength are applied to the antenna in order to calibrate the transducer and readout system.

III. NORMAL MODE TRANSFER FUNCTIONS

The model presented in this paper extends previous work by treating the coupled antenna-transducer as a single detector component possessing two degrees of freedom. In this way, we determine a transfer function describing the motion of the transducer (the observable motion) in terms of force applied to the bar (the physically interesting source). A second transfer function describes the motion of the transducer in terms of a force applied directly to the transducer (a dominant noise source). A third transfer function, describing the calibration procedure, describes the motion of the antenna face in terms of the force applied to the antenna.

The ideal detector is built from an antenna and resonator with identical resonant frequencies. In practice, perfect tuning between the components is nearly impossible to achieve. The normal mode description of detector operation combines the effects of imperfect tuning into a single parameter common to all of the transfer functions. By combining the normal mode solution for the coupled antenna-transducer with the impedance matrix calibration procedure of Boughn *et al.*, we obtain several new results. We explain how mistuning between the antenna and transducer causes the different responses observed during calibration of the force generator. We show how this measurement allows the mistuning parameter and the effective mass of the transducer to be experimentally determined, and we quantify the effects of mistuning on signal propagation and detector noise processes.

At this point, the following conventions are adopted and used throughout this paper. $\tilde{X}$ represents the Fourier transform of $X(t)$. The Fourier transform of an external force applied to the bar is represented by $\tilde{F}_1$. In this context, external means any force not created by the antenna-transducer interaction. $\tilde{F}_2$ represents an external force applied directly to the transducer. $\tilde{x}_1$ represents the inertial displacement of the bar resulting from $\tilde{F}_1$ and/or $\tilde{F}_2$, and $\tilde{x}_2$ represents the

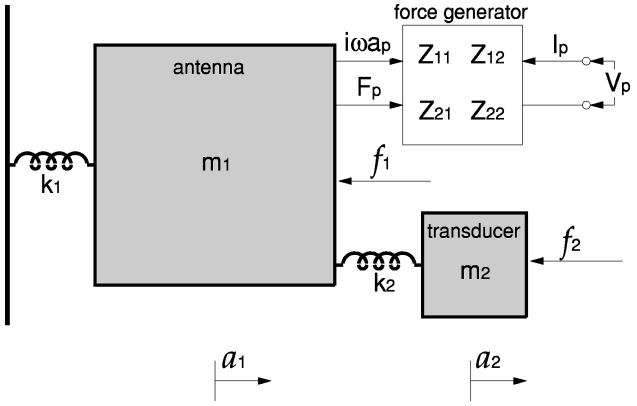

FIG. 2. The two-mass and two-spring model of a gravitational wave antenna and resonant transducer, including a two-port representation of the force generator.

inertial displacement of the transducer resulting from $\tilde{F}_1$ and/or $\tilde{F}_2$. Also, from this point on, since all of the physically interesting motion of the system is longitudinal, the equations of motion are written in one dimension.

The coupled oscillator model of an antenna and resonator, assuming that damping is small enough to be ignored, is pictured schematically in Fig. 2. In terms of mass-normalized coordinates, defined by $\mathbf{x}=\mathbf{M}\mathbf{u}$, where

$$\mathbf{M}=\begin{bmatrix} \dfrac{1}{\sqrt{m_1}} & 0 \\ 0 & \dfrac{1}{\sqrt{m_2}} \end{bmatrix}, \tag{3}$$

the equations of motion of the coupled oscillators are

$$\ddot{\mathbf{u}}=-\mathbf{K}\mathbf{u}+\mathbf{M}\mathbf{F}. \tag{4}$$

The displacement of the antenna face is given by u_1. The displacement of the transducer is given by u_2. The matrix $\mathbf{K}$, called the mass-normalized elastic matrix, is equal to

$$\mathbf{K}=\begin{bmatrix} -\left(\omega_1^2+\dfrac{m_2}{m_1}\omega_2^2\right) & \sqrt{\dfrac{m_2}{m_1}}\,\omega_2^2 \\ \sqrt{\dfrac{m_2}{m_1}}\,\omega_2^2 & -\omega_2^2 \end{bmatrix}, \tag{5}$$

where $\omega_2=k_2/m_2$ is the uncoupled resonant frequency of the resonator. $\mathbf{F}$ contains the external forces acting on the system,

$$\mathbf{F}=\begin{bmatrix} F_1 \\ F_2 \end{bmatrix}. \tag{6}$$

Since the matrix $\mathbf{K}$ is both real and symmetric, we can rewrite Eq. (4) in terms of normal coordinates. The transformation from mass-normalized coordinates to normal coordinates is a rotation; we denote the rotation matrix as $\mathbf{A}$. Math-

ematically, the matrix **A** diagonalizes the matrix **K** so that $\mathbf{KA}=\mathbf{AD}$, where **D** is the diagonal matrix of eigenfrequencies,

$$\mathbf{D}=\begin{bmatrix}\omega_+^2 & 0\\ 0 & \omega_-^2\end{bmatrix}. \tag{7}$$

Since this system has two degrees of freedom, the rotation **A** is characterized by a single parameter θ, the ''mixing-angle,''

$$\mathbf{A}=\begin{bmatrix}\cos\theta & \sin\theta\\ -\sin\theta & \cos\theta\end{bmatrix}. \tag{8}$$

The relationships between the inertial parameters and normal mode parameters of a two-mass–two-spring model are obtained from the matrix form of the equation $\mathbf{K}=\mathbf{ADA}^{-1}$,

$$\begin{bmatrix}-\left(\omega_1^2+\frac{m_2}{m_1}\omega_2^2\right) & \sqrt{\frac{m_2}{m_1}}\omega_2^2\\ \sqrt{\frac{m_2}{m_1}}\omega_2^2 & -\omega_2^2\end{bmatrix}$$
$$=\begin{bmatrix}-\omega_+^2\cos^2\theta-\omega_-^2\sin^2\theta & (\omega_+^2-\omega_-^2)\sin\theta\cos\theta\\ (\omega_+^2-\omega_-^2)\sin\theta\cos\theta & -\omega_+^2\sin^2\theta-\omega_-^2\cos^2\theta\end{bmatrix}. \tag{9}$$

The value of m_1 has been independently measured, leaving three unknowns in the left side of Eq. (9). Solutions of Eq. (9) reveal that the value of the mixing angle depends upon both the frequency difference and mass ratio of the bare antenna and the bare transducer. Perfect tuning, where both modes behave identically except for a difference in phase, corresponds to the coupling of a finite mass to an infinitesimal mass of an identical resonant frequency. The mixing angle in this case is 45°. If the current version of ALLEGRO was constructed from an antenna and transducer of identical frequencies $\omega_1=\omega_2\approx 900$ Hz, the finite mass ratio $m_1/m_2\approx 1800$ would produce a mixing angle of 44.7°, a very good approximation to perfect tuning. In reality, the approximately 12 Hz frequency difference between components of ALLEGRO in combination with the finite mass ratio leads to a mixing angle of approximately 30°.

In terms of the mass-normalized coordinates, the normal coordinates for the coupled oscillator system are $\mathbf{y}=\mathbf{A}^T\mathbf{u}$, where $\mathbf{A}^T$ denotes the transpose of the matrix **A**. Each component of **y** satisfies a harmonic oscillator equation [20]. Using a Fourier transformation, we rewrite the rotated version of Eq. (4) as an algebraic equation, $\tilde{\mathbf{y}}=\mathbf{\Delta A}^T\mathbf{M}\tilde{\mathbf{F}}$, where the matrix $\mathbf{\Delta}$ is the diagonal matrix of harmonic oscillator response functions,

$$\mathbf{\Delta}=\begin{bmatrix}\frac{1}{\omega_+^2-\omega^2} & 0\\ 0 & \frac{1}{\omega_-^2-\omega^2}\end{bmatrix}. \tag{10}$$

Transforming back to the inertial coordinates measured by the readout system, $\tilde{\mathbf{x}}=\mathbf{MA}\tilde{\mathbf{y}}$, the response of either mass to a set of externally applied forces is

$$\tilde{\mathbf{x}}=\mathbf{MA\Delta A}^T\mathbf{M}\tilde{\mathbf{F}}. \tag{11}$$

The utility of Eq. (11) is most obvious when it is rewritten in matrix form. The five-matrix product $\mathbf{MA\Delta A}^T\mathbf{M}$ is equal to a single 2×2 matrix. We denote this matrix as **G**, where

$$\begin{bmatrix}\tilde{x}_1\\ \tilde{x}_2\end{bmatrix}=\begin{bmatrix}G_{11} & G_{12}\\ G_{21} & G_{22}\end{bmatrix}\begin{bmatrix}\tilde{F}_1\\ \tilde{F}_2\end{bmatrix}. \tag{12}$$

Expressed in terms of m_1, m_2, ω_+, ω_-, and θ, the matrix elements are

$$G_{11}=\frac{\cos^2\theta}{m_1(\omega_+^2-\omega^2)}+\frac{\sin^2\theta}{m_1(\omega_-^2-\omega^2)}, \tag{13}$$

$$G_{12}=G_{21}=\frac{-\sin\theta\cos\theta}{\sqrt{m_1m_2}(\omega_+^2-\omega^2)}+\frac{\sin\theta\cos\theta}{\sqrt{m_1m_2}(\omega_-^2-\omega^2)}, \tag{14}$$

$$G_{22}=\frac{\sin^2\theta}{m_2(\omega_+^2-\omega^2)}+\frac{\cos^2\theta}{m_2(\omega_-^2-\omega^2)}. \tag{15}$$

Each matrix element in Eq. (12) is a transfer function describing the displacement of the antenna or transducer in terms of externally applied forces. Each transfer function is a superposition of the response at the two mode frequencies. The motion of either mass is a superposition of responses from forces applied at the two driving points.

IV. DRIVING POINT RESPONSE

The driving point response of the detector describes the motion of the *face of the antenna* in response to a force applied to the antenna. The driving point response is important because a resonant mass gravitational wave antenna is calibrated by applying forces to the antenna face using the force generator. The transfer function which describes the driving point response is G_{11}. The force on the antenna is equal and opposite to F_p, the force caused by the force generator, so that $\tilde{F}_1=-\tilde{F}_p$ (the sign difference arises from a standard convention that power flows into the force generator [21]),

$$\tilde{x}_1=\left(\frac{\cos^2\theta}{m_1(\omega_+^2-\omega^2)}+\frac{\sin^2\theta}{m_1(\omega_-^2-\omega^2)}\right)(-\tilde{F}_p). \tag{16}$$

Calibration in this manner requires accurate determination of the generator constant, which is the ratio between voltage applied to the capacitor and resulting force applied to the antenna. Boughn *et al.* showed how the energy-coupling coefficient between force generator and antenna can be determined through use of the reciprocity relation connecting the ''sending'' and ''receiving'' modes of transducer operation. This method has the advantages that it can be performed *in situ* and that it requires only straightforward electrical mea-

surements. In what follows, we present a detailed account showing how inclusion of the normal-mode model of the antenna improves the utility of the procedure developed by Boughn *et al.* The improved antenna-transducer model allows measurement of the mixing angle and of the force-to-voltage constant of the force generator.

A complete yet compact way to combine the normal-mode picture of the antenna and transducer with the behavior of the force generator is with an impedance matrix representation [21]. In this representation, the force generator is described in terms of the currents and voltages passing through an electrical port, and the forces and velocities at a mechanical port. The antenna-transducer system is a load terminating the mechanical port. The impedance matrix relates voltage $\tilde{V}_p$ and current $\tilde{I}_p$ to force $\tilde{F}_p$ and velocity $i\omega\tilde{x}_p$. These quantities are chosen since, at either end, their product is the power passing through the port. We note that when operated with a small ac voltage applied in addition to a constant dc voltage, the capacitive force generator is a linear device. In the Fourier domain,

$$\begin{bmatrix} \tilde{F}_p \\ \tilde{V}_p \end{bmatrix} = \begin{bmatrix} Z_{11} & Z_{12} \\ Z_{21} & Z_{22} \end{bmatrix} \begin{bmatrix} i\omega\tilde{x}_p \\ \tilde{I}_p \end{bmatrix}. \tag{17}$$

The Z_{ij}'s are rational polynomials which can be represented in terms of poles and zeros. For a broad class of transducers, including the force generator mounted on ALLEGRO, $Z_{12} = -Z_{21}^*$. Since we ignore losses, this implies $Z_{12} = Z_{21}$.

When a voltage is applied to the force generator, the response of the antenna face is (see the Appendix for the proof of this)

$$\tilde{x}_1 = \left(\frac{\cos^2\theta}{m_1(\omega_+^2 - \omega^2)} - \frac{\sin^2\theta}{m_1(\omega_-^2 - \omega^2)} \right) \left(\frac{-Z_{12}}{Z_{22}} \right) \tilde{V}_p. \tag{18}$$

Equation (18) implies that the amount of force applied to the antenna is given by the product of $\tilde{V}_p$ and Z_{12}/Z_{22}. The ratio Z_{12}/Z_{22} evaluated at $\omega_\pm$, which we denote as $\mathcal{Z}(\omega_\pm)$, is the voltage to force constant of the force generator at $\omega_\pm$,

$$F_p(t) = \mathcal{Z}(\omega_\pm) V_p(t). \tag{19}$$

The time domain response of the antenna face, $x_1(t)$, is given by the convolution of the system's impulse response with $V_p(t)$. The impulse response of the force generator-antenna-transducer combination, which we denote as $R(t)$, is the inverse Fourier transform of the product of the first two factors on the right side of Eq. (18),

$$R(t) = \frac{1}{m_1} \left(\frac{\mathcal{Z}(\omega_+)\cos^2\theta}{\omega_+} \sin(\omega_+ t) + \frac{\mathcal{Z}(\omega_-)\sin^2\theta}{\omega_-} \sin(\omega_- t) \right). \tag{20}$$

For a sinusoidal voltage of amplitude V_0 and duration T, the antenna's response (at times greater than T) is

$$x_1(t) = \int_0^T V_0 \sin(\omega_+ t') R(t - t') dt'. \tag{21}$$

Assuming that losses in the force generator are negligible, the amplitude of the antenna face in response to a wave train at ω_+ is

$$x_1(t) = \frac{V_0 T \mathcal{Z}(\omega_+)\cos^2\theta}{m_1 \omega_+} \cos(\omega_+ t). \tag{22}$$

For a driving force at ω_-, the response is

$$x_1(t) = \frac{V_0 T \mathcal{Z}(\omega_-)\sin^2\theta}{m_1 \omega_-} \cos(\omega_- t). \tag{23}$$

Equations (22) and (23) imply that a sinusoidal voltage applied to the force generator at either resonance frequency sends the antenna face into simple harmonic motion.

When the driving voltage is disconnected and the force generator is shorted, the oscillations of the antenna face drive a current through the electrical port of the force generator. The driving oscillation is given by Eq. (22) after an excitation of the plus mode and by Eq. (23) after an excitation of the minus mode. The current passing through the electrical port is given by solving Eq. (17) with $\tilde{V}_p = 0$. The amplitude of this current in the time domain is determined by taking the inverse Fourier transform of the result. When the driving term $\tilde{x}_1$ is monochromatic, $I_{p\pm}(t)$ is

$$I_{p\pm}(t) = \mathcal{Z}(\omega_\pm)\dot{x}_1(t). \tag{24}$$

Substituting Eq. (22) into the above equation, functions for $I_{p\pm}(t)$ for each mode are obtained:

$$I_{p+}(t) = \frac{V_0 T \mathcal{Z}^2(\omega_+)\cos^2\theta}{m_1} \sin(\omega_+ t), \tag{25}$$

$$I_{p-}(t) = \frac{V_0 T \mathcal{Z}^2(\omega_-)\sin^2\theta}{m_1} \sin(\omega_- t). \tag{26}$$

To concisely express the relationships between the measurements and the model, the directly measured quantities (V_0, T, the amplitude of $I_{p\pm}$) are combined into a single parameter for each mode labeled γ_+ and γ_-,

$$\gamma_\pm = \left(-\frac{I_{0\pm}}{V_0 T} \right). \tag{27}$$

By substituting γ_+ and γ_- into Eqs. (25) and (26) the relationships between the mode responses of ALLEGRO and the transfer function parameters are

$$\gamma_+ = \frac{\mathcal{Z}^2(\omega_+)\cos^2\theta}{m_1}, \tag{28}$$

$$\gamma_- = \frac{\mathcal{Z}^2(\omega_-)\sin^2\theta}{m_1}. \tag{29}$$

The differences between γ_+ and γ_- observed in both the Stanford detector and ALLEGRO are thus explained as a function of the mechanical mistuning. Since $\mathcal{Z}(\omega_+)$ and $\mathcal{Z}(\omega_-)$ should be equal, the mode amplitudes are equal only when $\theta \approx 45°$. If the antenna and transducer have different uncoupled resonant frequencies, this condition is not true.

V. SIGNAL RESPONSE

In this section, we consider the response of the detector to a signal. The signal response of the detector describes the motion of the *transducer* in response to a force applied to the antenna. Driving the antenna with a gravity wave is an excitation where $F_{sig}(t)=F_1(t) \gg F_2(t)$ over the duration of the signal. The motion detected by the readout system is a voltage proportional to the differential displacement of the resonator, $x_2(t)-x_1(t)$. Since $m_1 \gg m_2$, this response is dominated by the transfer function G_{21},

$$\tilde{x}_2=\left(\frac{-\sin\theta\cos\theta}{\sqrt{m_1 m_2}(\omega_+^2-\omega^2)}+\frac{\sin\theta\cos\theta}{\sqrt{m_1 m_2}(\omega_-^2-\omega^2)}\right)\tilde{F}_{sig}. \tag{30}$$

Comparing Eq. (30) to the Fourier transform of Eq. (2) shows how much is gained by the addition of a resonant transducer. For a bare bar, the response to a signal in the Fourier domain is

$$\tilde{x}_1=\frac{1}{m_1(\omega_1^2-\omega^2)}\tilde{F}_{sig}. \tag{31}$$

Comparing Eq. (31) to Eq. (30) illustrates the mechanical gain resulting from use of a resonant transducer. The amplitude of oscillation of each mode of the transducer is a factor of $\sqrt{m_1/m_2}\sin\theta\cos\theta$ larger than the amplitude of a bare bar. In either mode, the maximum gain occurs when $\theta \approx 45°$, so that $\sin\theta\cos\theta=.5$. As the two modes beat in and out of phase, the maximum displacement of the transducer is the sum of the maximum displacements of the individual modes. For ALLEGRO, the maximum gain is $\sqrt{m_1/m_2}$, approximately a factor of 40.

This equivalence of the θ dependent factor in the plus and minus mode terms implies that an excitation of the bar produces approximately equal mode amplitudes, regardless of any mistuning between the bar and the transducer. This unambiguous prediction of the model is an important diagnostic. If the motion of resonant bar gravitational wave antennas is truly that of coupled harmonic oscillators, both modes must respond to broadband excitations with equal amplitudes. This is a test to see if the system has been constructed properly, as well as a veto criteria for eliminating spurious events during operation.

For purposes of calibration, a gravity wave is mimicked by applying a short-duration voltage, or calibration pulse, to the force generator. The voltage produces an impulse on each of the detector's resonant modes. The effect of the impulse on the motion of the transducer is measured using the demodulation scheme shown in Fig. 3. The voltage output of the detector is mixed with a reference signal between frequencies ω_+ and ω_-, moving the information contained in the resonant modes into a frequency band centered at dc. After being passed through an anti-aliasing filter, the voltage is then sampled every 8 ms. The now digitized signal is mixed with a reference signal that moves one of the resonant modes to zero frequency. This dc signal is digitally filtered to optimize the signal to noise ratio [4]. The same procedure is repeated for the other mode. The digital filter is optimized for identifying sudden changes in the sampled output voltage.

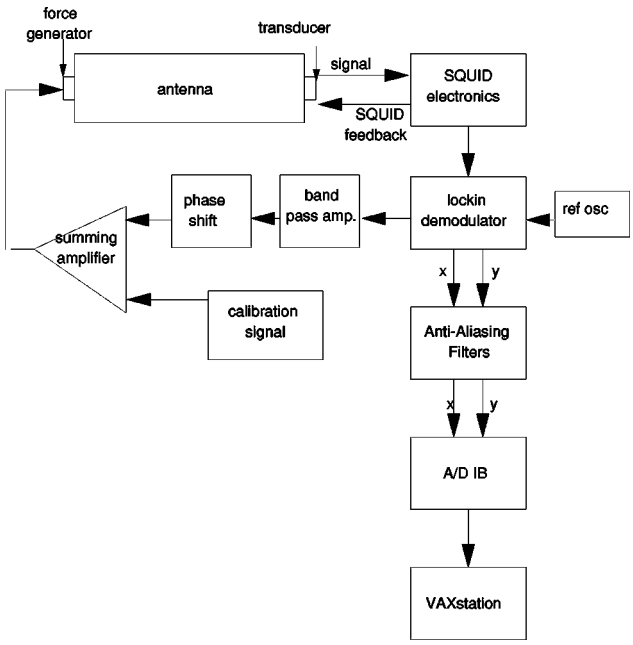

FIG. 3. Block diagram of the demodulation and readout scheme used to acquire ALLEGRO data.

This procedure is best understood by noting that a short-duration impulse causes a sudden change in the amplitude and phase of the Brownian-driven oscillations of the bar. This is reflected in a sudden change in the amplitude and phase of the motion of the transducer. The demodulation scheme divides the real-valued oscillations of the antenna into in-phase and quadrature components measured with respect to the reference signal. The amplitudes of the in-phase and quadrature channels contain all of the magnitude and phase information about the original time-domain signal [22]. Between any two samples, the change in amplitude of the in-phase component is proportional to the Fourier sine transform of the driving force on the oscillator at that instant, while the change in amplitude of the quadrature component is equal to the Fourier cosine transform of the driving force. We define the complex sum of the components as the complex amplitude. By looking for sudden changes in the complex voltage amplitude of the transducer's oscillations with the digital filter, both the magnitude and the phase of the transducer's time-domain oscillations are used in detecting a signal.

At each sampling time, the output of the digital filter is a discrete number of bits (referred to as digital units). The exact number of digital units produced when the antenna is excited depends on the antenna-transducer transfer function,

the analog to digital conversion, and any gains introduced during demodulation and filtering. By applying calibration pulses of different voltages, we determine that the number of digital units produced varies linearly with the voltage applied to the force generator. We are also able to determine the constant of proportionality between voltage applied with the force generator and digital units measured at the readout system. With the voltage-to-digital unit constant known, we use Eq. (19) to normalize the output from the readout system in terms of force applied to the antenna.

Ultimately, we wish to normalize the output of the readout system in terms of the strength of an incident gravity wave. In the frequency domain, the force applied to the antenna by an interaction with a gravity wave is given by the Fourier transform of Eq. (1),

$$\tilde{F}_G(\omega) = -\frac{1}{2} m_1 l_1 \omega^2 \tilde{h}(\omega), \tag{32}$$

where $\tilde{h}(\omega)$ is the Fourier transform of the dimensionless strain of the gravity wave signal, and l_1 is the effective length of the antenna. For the purpose of calibration, it is convenient to define a standard reference signal [9]. A candidate event is assigned the amplitude that is produced by a single cycle of a sine wave at the frequency where it is detected. The Fourier components of the reference signal are

$$\tilde{h}(\omega_\pm) = \frac{\pi h_G}{\omega_\pm}, \tag{33}$$

where h_G is the amplitude of the reference signal. Combining Eqs. (19), (32) and (33), the digital output of the detector can be normalized in terms of dimensionless strain. Given that we measure D_{cal} digital units in response to a single-cycle calibration pulse of V_{cal} volts (zero-to-peak), we assign a burst amplitude of

$$h_G = \sqrt{\frac{2\mathcal{Z}(\omega_\pm) V_{cal}}{\omega_\pm^2 m_1 l_1}} \left(\frac{D_{obs}}{D_{cal}} \right), \tag{34}$$

to an output of D_{obs} digital units observed at the readout system.

Although the force applied to each mode by a broadband signal is roughly equal, the energy deposited into each mode is not. This is physically explained by considering the transfer of energy between coupled oscillators. A complete transfer of energy between two coupled oscillators occurs only in a perfectly tuned system. If the oscillators are not perfectly tuned, only a portion of the energy is transferred. Since the signal readout depends primarily on the motion of the smaller mass transducer, the observable quantities contain only a fraction of the total energy deposited in the system.

In normal coordinates, the energy present in a two-mass–two-spring system is $E = \dot{\mathbf{y}}^T \dot{\mathbf{y}}/2 + \mathbf{y}^T \mathbf{D} \mathbf{y}/2$. In terms of a detector's physical parameters, the energy deposited in the system by a gravity wave of finite duration is

$$E = \frac{1}{8} m_1 l_1^2 [|\tilde{h}(\omega_+)|^2 \omega_+^4 \cos^2\theta + |\tilde{h}(\omega_-)|^2 \omega_-^4 \sin^2\theta]. \tag{35}$$

This result implies that some caution must be exercised in interpreting signal strength conventions which refer to energy. Established burst energy conventions treat the two modes of the detector as two independent antennas and the response of either antenna to a signal is assumed to be identical. Equation (35) shows that this is not the case. Any broadband excitation deposits different amounts of energy into each mode of a mistuned detector. The energy deposited into an individual mode cannot be assigned unless the mistuning parameter is known. By using the strain convention defined in Eq. (34), derived from considering the force applied to the detector, the strength of a gravity wave is expressed for either individual detector mode without any reference to antenna dependent mistuning.

VI. TRANSDUCER FORCE NOISE RESPONSE

Experiments on early generations of inductive transducers, as well as on the ALLEGRO system, confirm that there are two separate sources of dissipation in the transducer that contribute to noise. According to the fluctuation-dissipation theorem, thermal noise generated in the transducer is related to losses inversely proportional to its mechanical quality factor. A second source of dissipation results from electrical losses that occur in the transducer (in spite of the fact that the system is superconducting). The specific mechanism behind the electrical losses is not well understood. These two sources of noise, the result of forces acting directly on the transducer, are called transducer force noise. At the detector's resonant frequencies, the transducer force noise is much greater than the noise originating in the dc SQUID amplifier. The SQUID white noise, added in series to the output of the transducer, is the dominant noise source off-resonance.

The transducer force noise response describes the motion of the transducer in response to forces applied directly to the transducer. The forces acting on the transducer are modeled as a series of stochastic impulses $F_2(t) = F_n(t)$. The spectral density of $F_n(t)$, denoted by $S_{nn}(\omega)$, is white. Stochastic forces within the antenna are neglected because it has been experimentally determined that the transducer is much more lossy than the antenna. Stochastic forces from the transducer on the antenna can be neglected because the inertial motion of the antenna is smaller due to its larger mass. The transducer force noise response is described by the transfer function G_{22}.

Since the decay time of either mode is on the order of tens or hundreds of seconds, the effects of damping cannot be neglected when considering noise. The effects of damping are considered by including an imaginary damping term in the denominator of G_{22},

$$\tilde{x}_2 = \left(\frac{\sin^2\theta}{m_2\left(\omega_+^2 + \frac{i\omega}{\tau_+} - \omega^2 \right)} + \frac{\cos^2\theta}{m_2\left(\omega_-^2 + \frac{i\omega}{\tau_-} - \omega^2 \right)} \right) \tilde{F}_n . \tag{36}$$

The size of the damping term is inversely proportional to the measured decay time of the mode. The decay times can be experimentally determined by observing the mode amplitudes for several minutes after they are excited with a large impulse. For ALLEGRO, the plus mode has a decay time of $\tau_+ \approx 80\,\mathrm{s}$, and the minus mode has a decay time of $\tau_- \approx 50\,\mathrm{s}$. The spectral density of the noise driven oscillations of the transducer is given by

$$S_{22}(\omega) = \frac{\sin^4\theta}{m_2^2} \frac{S_{nn}(\omega)}{(\omega^2-\omega_+^2)^2+\frac{\omega^2}{\tau_+^2}} + \frac{\cos^4\theta}{m_2^2} \frac{S_{nn}(\omega)}{(\omega^2-\omega_-^2)^2+\frac{\omega^2}{\tau_-^2}}. \tag{37}$$

The spectral density at a mode frequency is measured by constructing the autocorrelation function of the transducer output. The autocorrelation function of $x_2(t)$ is defined as the expectation value of the product $x_2(t)x_2(t-t')$. By the Wiener-Khintchin theorem, the autocorrelation function is equal to the inverse Fourier transform of the power spectrum of a stochastic process. If a passband filter is applied to the output of the transducer so that only data near the plus mode is kept, $\langle x_2(t)x_2(t-t')\rangle$ is equal to the inverse Fourier transform of the the first term of the right-hand side of Eq. (37). Evaluating this expression at $t'=0$ [23],

$$\langle x^2(t)\rangle_+ = \frac{S_{nn}(\omega_+)\tau_+ \sin^4\theta}{2m_2^2\omega_+^2}. \tag{38}$$

Similarly, for data from the minus mode,

$$\langle x^2(t)\rangle_- = \frac{S_{nn}(\omega_-)\tau_- \cos^4\theta}{2m_2^2\omega_-^2}. \tag{39}$$

By definition, the autocorrelation function evaluated at $t'=0$ is the mean-squared value of the transducer's displacement. Although both modes are driven by the same stochastic force, we expect to observe different mean-squared displacements of the modes in the absence of any large impulses. Since the signal response of both modes is equal, this implies that one mode is more sensitive than the other in a mistuned system.

It should be noted that the magnitude of the mean squared displacement of the transducer can be calculated using the equipartition theorem if both modes are allowed to freely decay. However, in actual operation, detectors using inductive transducers are run with constant feedback from the SQUID applied to the antenna face via the force generator to avoid instabilities. The feedback causes the decay time in each mode to be different, and the conditions for the equipartition theorem do not hold.

Equations (38) and (39) add to our diagnostic tools. The ratio of the two autocorrelation functions provides a second measure of the mixing angle, providing a test of the consistency of the model. Knowing the mixing angle, the magnitudes of the autocorrelation functions provide another measure of how close our system is to being limited by the fundamental noise sources predicted by the fluctuation-dissipation theorem.

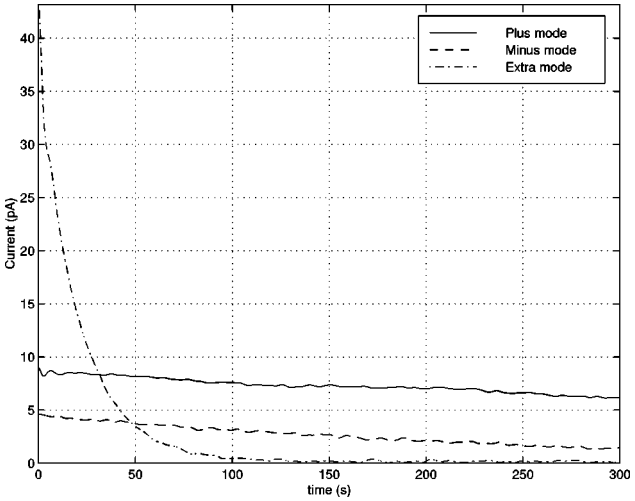

FIG. 4. Current measured through the force generator versus time after the antenna has been excited with a 25-s wave train through the force generator.

VII. EXPERIMENTAL RESULTS AND DISCUSSION

In this section, we briefly review the procedure and then present the different ALLEGRO outputs relating to the normal mode transfer functions. The presentation of the data makes apparent the fact that the ALLEGRO system possesses a third resonant mode. In addition to its two designed modes at 895.414 Hz and 919.659 Hz, ALLEGRO has a third mode with a resonant frequency of 887.742 Hz. First, we attempt to explain the results with a purely two-mode model, but show that this explanation is incomplete. By extending the model, it is possible to identify the physical location of the extra mode and make quantitative predictions of its effect.

The driving point response for each mode, including the extra mode, was measured by the procedure described in Sec. IV. In three separate measurements, 25-s wave trains of 20 volts zero-to-peak were applied (in addition to 150 dc volts) to the plus mode, minus mode, and extra mode. Immediately after, the current driven through the force generator was measured with a lock-in amplifier. Figure 4 shows a plot of the amplitude of the current versus time for each measurement. The ratio of current measured at the plus mode to the minus mode was approximately 2 to 1. The extra mode shows the largest response, nearly an order of magnitude larger than the response of the minus mode.

The signal response of ALLEGRO was measured by applying one cycle of a sine wave of 2.0 V peak-to-peak to the antenna with the force generator. Figure 5 shows spectra of 20-s intervals of ALLEGRO's output before and after the impulse was applied to the bar. Figure 6 shows several cycles of ALLEGRO's demodulated output acquired immediately after the impulse was applied. The data have been shifted in frequency to produce a graph of the real-time re-

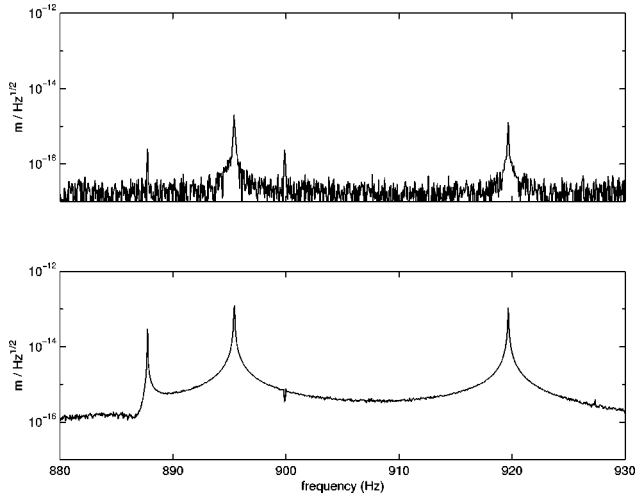

FIG. 5. The spectral density of ALLEGRO's output (a) before a ''calibration pulse'' or artificial gravity wave is applied and (b) after a calibration pulse is applied. These plots clearly show the presence of a third mode near 887.7 Hz.

sponse of the detector. Three sine waves, shown in Fig. 7, are required to reconstruct this signal. The frequencies, amplitudes, and decay constants of the fitted waves were extracted from the data using a lock-in amplifier. The only free parameter is the initial starting time. Subtracting these three sine waves from the actual data shows that these three frequency components account for most of ALLEGRO's response to a burst.

It is important to note that Eq. (30) predicts that the plus and minus mode amplitudes should be equal immediately after the bar is hit with a large impulse. ALLEGRO does not show this behavior. After the impulse has been applied, the amplitude of the minus mode is consistently larger than the amplitude of the plus mode. Repeated measurements made immediately after exciting the antenna show that the plus mode has only (0.82 ± 0.03) percent of the amplitude of the minus mode. This result will be explained later.

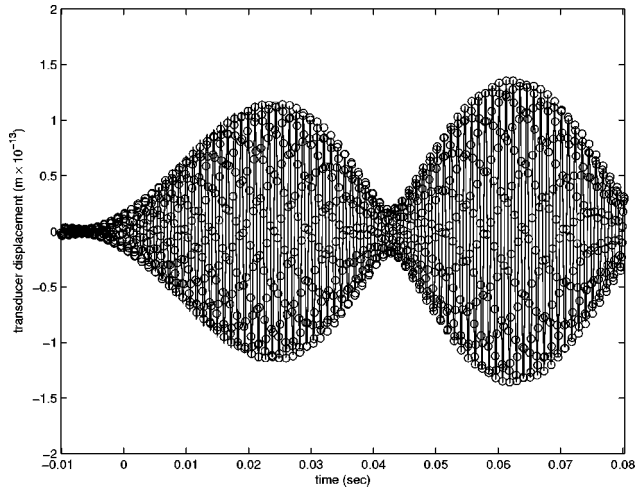

FIG. 6. The real-time response of ALLEGRO to an applied impulse. The solid line is actual data. The circles are the result of a fit.

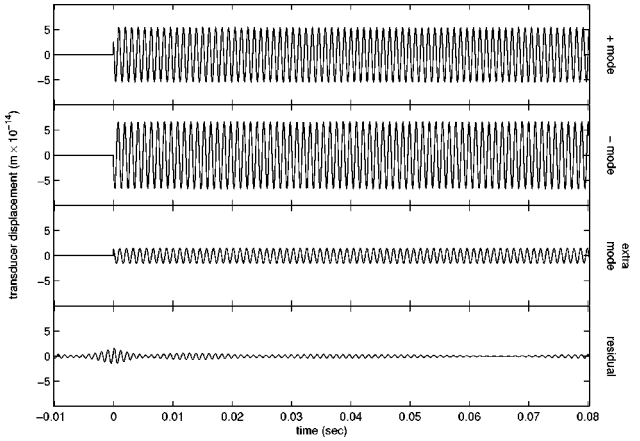

FIG. 7. (a), (b), and (c) are the fitted components of ALLEGRO's response to an impulse extracted from the data. These three sine waves were subtracted from Fig. 6, producing the residuals shown in plot (d).

First, we note that the digital filtering does work as designed. Using the force generator, single cycle calibration pulses with voltages of 1.0, 2.0, and 3.0 V and frequency 907.53 Hz were applied approximately 10 s apart from one another (this is equal to applying dimensionless strains of 3.3×10^{-16}, 6.5×10^{-16}, and 9.8×10^{-16} to the bar). The top half of Fig. 8 shows the samples of the in-phase channel of demodulated transducer voltage. The bottom half of Fig. 8 shows the corresponding filtered output of the minus mode. The filtered output is a maximum at the samples corresponding the times when pulses were applied, and the heights of the peaks are proportional to the applied voltage. Figure 8 demonstrates that the filter responds to a sudden change in mode amplitude, not simply to the size of the voltage amplitude.

Figure 9 is a plot of the in-phase versus quadrature mode amplitudes for the plus mode for the calibration pulses applied in Fig. 8. Initially, the antenna was at rest, and the

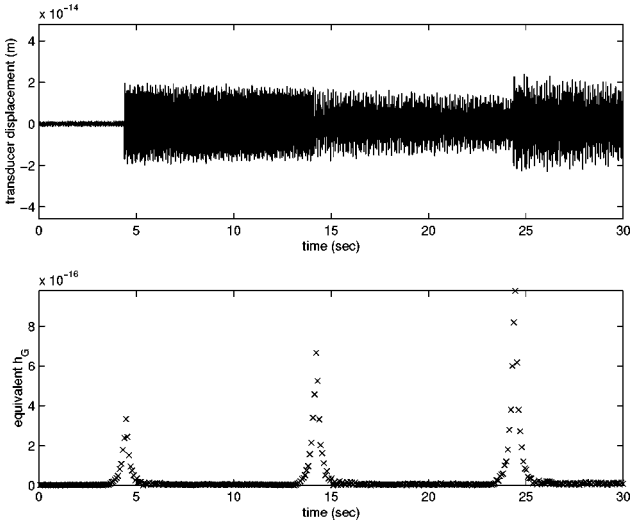

FIG. 8. Comparison of the digitized raw voltage output and digitally filtered output from ALLEGRO.

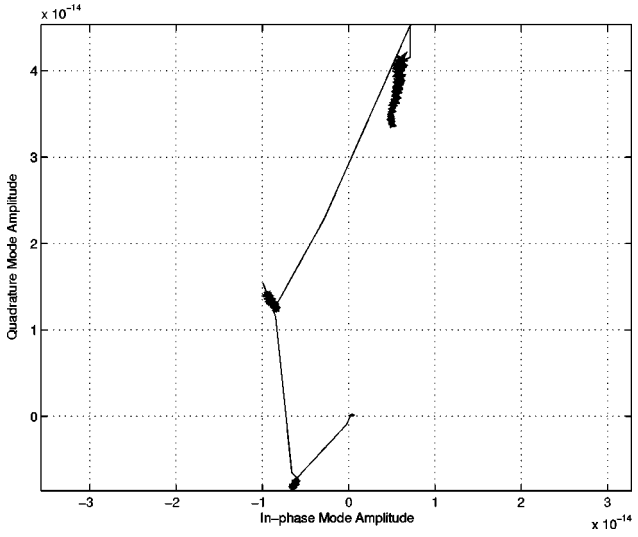

FIG. 9. A plot of the in-phase component versus the quadrature component of the minus mode for the data shown in Fig. 8. The height of the peak produced by the digital filter is proportional to the change in the mode amplitude.

amplitudes of both channels were nearly zero. When the 1.0-V pulse was applied, both amplitudes jumped. The amplitudes then very slowly began to decay towards zero until the 2.0-V pulse was applied. Even though the change in time-domain amplitude after the 2.0-V pulse was much smaller than the change in time-domain amplitude in response to the 1.0-V pulse (see Fig. 8), the digital filter still identified the second pulse as the larger of the two. This is because the filter responds to both the magnitude and phase of oscillation, contained completely in the amplitudes of the in-phase and quadrature channels. The change in complex amplitude goes linearly with force applied to the oscillator, which goes linearly with the voltage applied to the force generator. The height of the filtered output peaks is proportional to the magnitude of the jump in phase space.

Figure 10 shows measured autocorrelation functions for the plus and minus modes. These plots were generated using 1 day's worth of data (day 011 of 1998), decimated to a rate of one sample per second. There were no large burst events on this day. The absolute values on the y axis of both graphs are accurate to approximately 10% due to uncertainties in the parameters needed to find the digital units to transducer amplitude coefficient. The peak of each of these graphs is equal to the mean-squared displacement of the transducer in the absence of any large impulses applied to the bar.

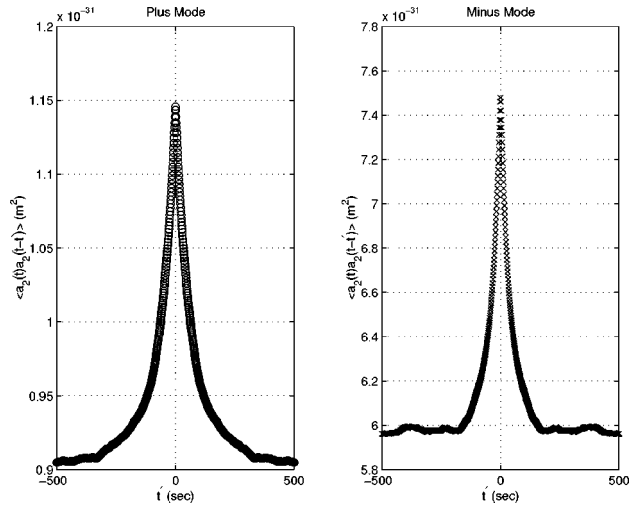

FIG. 10. Autocorrelation functions of ALLEGRO's noise on day 011 of 1998, a day when no large bursts occurred.

A. Two mode model

In a true two mode system, the measurement of the driving-point response of the two modes uniquely determines the values of the generator constant and the mixing angle. Solving Eqs. (28) and (29) assuming that $\mathcal{Z}(\omega_+)=\mathcal{Z}(\omega_-)$, the voltage-to-force constant and the mixing angle are

$$\tan\theta=\sqrt{\frac{\gamma_-}{\gamma_+}}, \tag{40}$$

$$\mathcal{Z}(\omega_\pm)=\sqrt{m_1(\gamma_++\gamma_-)}. \tag{41}$$

With known values for ω_+, ω_-, and θ, values for the uncoupled parameters ω_1, ω_2, and m_2 can be determined from Eq. (9). The left side of Eq. (9) is the model of the system's elastic behavior. The right side is a matrix of experimentally determined numbers. Since the value of m_1 has been independently measured, there are three equations for three unknowns. Using measured ALLEGRO values for γ_+ and γ_- (shown in Table I), Eq. (40) yields a mixing angle $\theta=36.0°$. Using this value for θ, Eq. (9) yields an uncoupled antenna frequency of $\omega_1=2\pi\times911.65\,\mathrm{rad\,s^{-1}}$, an uncoupled transducer frequency of $\omega_2=2\pi\times903.86\,\mathrm{rad\,s^{-1}}$, and a transducer effective mass of $m_2=0.75\,\mathrm{kg}$.

With known values for $\mathcal{Z}(\omega_\pm)$, θ, and m_2, the value of the sensor constant can be determined. The sensor constant is the constant of proportionality between the inertial displacement of the transducer measured in meters and the digital units of voltage recorded by the data acquisition system. From the relation $\tilde{x}_2=G_{21}\tilde{F}_1$, we know the amplitude of oscillation of the transducer for a given force applied to the antenna. From Eq. (19) we know the force applied to the bar for a given voltage. By combining these two relations, the oscillation of the transducer in response to N cycles of V_0 volts applied to the force generator is expressed in meters as

$$x_2(t)=\frac{\pi V_0 N\mathcal{Z}(\omega_\pm)\sin\theta\cos\theta}{\sqrt{m_1m_2}\omega_\pm^2}\cos(\omega_\pm t). \tag{42}$$

The transducer's digitally recorded amplitude of oscillation in response to a calibration pulse is normalized using Eq. (42).

The experimental results are not consistent with the two mode model. As stated before, the amplitude of the plus mode is only 0.82 that of the minus mode after an excitation. The model predicts that the amplitudes of excitation should differ only by the ratio of the mode frequencies, which differ only by approximately one percent. The large difference in

mode responses leads to different sensor constants for the plus and minus modes. This is physically unreasonable. Finally, the ratio of autocorrelation functions predicted by the ratio of Eq. (39) to Eq. (38) is 2.4 while the measured ratio is 6.5. The presence of the extra mode cannot be neglected.

B. Three mode model

There are two possible physical locations for the extra mode. It can either be an extra resonance in the antenna-transducer system of Eq. (12), or an extra resonance in the force generator of Eq. (17). Because the antenna-transducer-force generator system is mechanically isolated (and sealed in a cryogenic dewar), it is not feasible to apply forces directly to different parts of the hardware in order to determine the location of the resonance. In spite of this difficulty, there is ample evidence showing that the extra mode is due to a parasitic resonance in the force generator.

The key to isolating its location is the fact that the amplitude of the extra mode's driving point response is significantly larger than the amplitude of the driving point responses of the plus and minus modes while its signal response (the height of its peak in Fig. 5) is relatively small. No third mass and spring added to the antenna-transducer using reasonable effective masses and spring constants to describe the detector produces this behavior. Furthermore, an additional resonance added to the model of the antenna-transducer near the minus mode frequency lowers the amplitude of the minus mode relative to the amplitude of the plus mode; the observed fact is that the amplitude of the minus mode is always larger than the amplitude of the plus mode in response to an excitation. The large driving point response from the extra mode results from the fact that the current in Eq. (24) is being measured with an instrument which is resonant at the frequency of the extra mode. Finally, during the original assembly of ALLEGRO, a resonance was observed at approximately 865 Hz (at room temperature) after the force generator was mounted on the bar. Since resonant frequencies change as a function of temperature, it is not unlikely that this resonance moved upward towards the designed modes of the detector.

A resonance in the force generator implies that the value of $\mathcal{Z}(\omega)$ is not constant near the extra mode's resonant frequency; the behavior of the force generator must be described by a voltage-to-force *function* rather than a voltage-to-force *constant*. Qualitatively, the resonance in the force generator does not change how we describe the mechanical relationships between the plus and minus modes; it only changes the ratio of force generated to voltage applied when applying calibration signals. This is quantitatively demonstrated in the Appendix.

Although each mode now has its own voltage-to-force constant, the reciprocity relation still holds. The voltage-to-force function of the force generator is identical to its velocity-to-current function. The driving point responses of the modes are characterized by

$$\gamma_+ = \frac{\mathcal{Z}^2(\omega_+)}{m_1}(\cos^2\theta + \epsilon_1), \tag{43}$$

$$\gamma_- = \frac{\mathcal{Z}^2(\omega_-)}{m_1}(\sin^2\theta - \epsilon_1). \tag{44}$$

where ϵ_1 is a small correction term arising from the force generator's effect on the resonant behavior of the antenna (explained in detail in the Appendix). Since $\mathcal{Z}(\omega_+) \neq \mathcal{Z}(\omega_-)$, the voltage-to-force constant is not proportional to the square root of the sum of γ_+ and γ_-. There are now three unknowns involved in these two measurements, and additional information is required to complete the calibration.

The required information is the amplitude ratio of the modes read out at the transducer in response calibration pulse. The mode excitation observed at the transducer is directly proportional to the force applied, but because of the force generator resonance, each mode receives a different force in response to the same voltage pulse. P_+ and P_-, the amplitudes of the modes after an excitation, are proportional to

$$P_+ \propto \frac{-\mathcal{Z}(\omega_+)\sin\theta\cos\theta}{\sqrt{m_1 m_2}\omega_+}(1+\epsilon_2), \tag{45}$$

$$P_- \propto \frac{\mathcal{Z}(\omega_-)\sin\theta\cos\theta}{\sqrt{m_1 m_2}\omega_-}(1+\epsilon_2). \tag{46}$$

The ratio of Eqs. (45) and (46), using the measured values for P_+ and P_-, along with Eqs. (43) and (44), provide three equations for the three unknowns $\mathcal{Z}(\omega_+)$, $\mathcal{Z}(\omega_-)$, and θ.

The modified expressions for voltage-to-force constants and mixing angle due to the resonant force generator are

$$\mathcal{Z}(\omega_+) = \sqrt{m_1\left[\gamma_+ + \left(\frac{\omega_+ P_+}{\omega_- P_-}\right)^2 \gamma_-\right]}, \tag{47}$$

$$\mathcal{Z}(\omega_-) = \frac{\omega_- P_-}{\omega_+ P_+}\mathcal{Z}(\omega_+), \tag{48}$$

$$\tan\theta = \frac{\omega_+ P_+}{\omega_- P_-}\sqrt{\frac{\gamma_-}{\gamma_+}}. \tag{49}$$

Using the corrected value for the mixing angle, the uncoupled ALLEGRO parameters can be determined from Eq. (9). The results are shown in Table I. They are in good agreement with previous measurements made on the system [19].

With the generator constant determined, we normalize the output of the digital filter in terms of dimensionless strain created by the reference waveform defined in Sec. V. The sensitivity of either mode is defined by its noise amplitude, the average of a large number of filtered output samples in the absence of any abnormally large bursts. As the results from the two modes provide two independent estimates of the size of the signal, statistically combining them improves the accuracy of our estimate. The expected distributions for a two-mode detector and how to combine the results from the

TABLE I. Measured ALLEGRO parameters.

Antenna mass	$m_1 = 1148\,\mathrm{kg}$
Plus mode frequency	$\omega_+ = 2\pi \times (919.659\,\mathrm{Hz})$
Minus mode frequency	$\omega_- = 2\pi \times (895.414\,\mathrm{Hz})$
Extra mode frequency	$\omega_X = 2\pi \times (887.742\,\mathrm{Hz})$
	$\gamma_+ = (2.22 \pm 0.09) \times 10^{-14}$ mho/s
	$\gamma_- = (1.17 \pm 0.05) \times 10^{-14}$ mho/s
Plus/minus signal response ratio	$P_+ / P_- = 0.82 \pm 0.03$
Minus/extra signal response ratio	$P_- / P_X = 4.4 \pm 0.2$
Plus mode generator constant	$\mathcal{Z}(\omega_+) = (5.9 \pm 0.1) \times 10^{-6}$ N/V
Minus mode generator constant	$\mathcal{Z}(\omega_-) = (7.0 \pm 0.2) \times 10^{-6}$ N/V
Two-mode mixing angle	$\theta = (30.5 \pm 2.5)^{\circ}$
Uncoupled antenna frequency	$\omega_1 = (913.83 \pm 0.76)$ Hz
Uncoupled transducer frequency	$\omega_2 = (902.58 \pm 0.79)$ Hz
Transducer effective mass	$m_2 = (0.64 \pm 0.05)$ kg

different modes are discussed in detail elsewhere [4]. As of 1998, the average strain noise amplitude of ALLEGRO is 1×10^{-18}.

Using the modified expressions for mixing angle and voltage-to-force constant, Eq. (42) can be used to determine the sensor constant. In its current operating state, one digital unit of ALLEGRO output is equal to 1.1×10^{-17} m of transducer displacement. This same constant is calculated for both modes. Given the mechanical gain due to the transducer, this is equivalent to measuring a strain creating a displacement of 2.6×10^{-19} m with a bare bar.

The ratio of the mean-squared displacements is approximately 6.5, consistent with a mixing angle of 29.4°, within the experimental uncertainty of the driving point measurement of θ. Assuming that the noise force is given by the fluctuation-dissipation theorem, this driving force has a spectral density of $S_{nn}(\omega) = 4k_b T m_2 \omega_{\pm} / Q_2$, where Q_2 is the mechanical quality factor of the transducer, equal to approximately 1.5×10^6, and T is the physical temperature of the bar, 4.2 K. Given the set of antenna parameters determined from the three-mode model, Eqs. (38) and (39) predict values of $1.2 \times 10^{-31}\,\mathrm{m}^2$ in the plus mode and $6.0 \times 10^{-31}\,\mathrm{m}^2$ in the minus mode. The measured values are within the experimental uncertainty determined by uncertainties in the mixing angle and the quality factor of the transducer.

VIII. STRAIN-NOISE SPECTRUM

Finally, we present the current sensitivity of the ALLEGRO detector. A useful way to characterize the sensitivity of a gravity wave detector is to determine its equivalent input strain noise. A plot of the equivalent input strain noise displays the noise of the detector in terms of the quantity that the detector is designed to measure, the strain of a passing gravitational wave. The equivalent input strain noise is the gravity wave spectrum that would produce the observed output spectrum in a noiseless detector.

The most straightforward way to calculate the strain noise spectrum is to divide the output noise spectrum by the signal transfer function. Experimentally, the signal transfer function can be determined by measuring the output spectrum of the detector while applying white voltage noise to the force generator. Because of the resonance in the force generator, the white voltage noise produces different forces at different frequencies. By combining Eq. (32) with the force generator's transfer function [Eq. (A28), derived in the Appendix], we determine the spectrum of input strain created by the white noise. The output spectrum (in digital units/$\sqrt{\mathrm{Hz}}$) divided by the input strain spectrum (in strain/$\sqrt{\mathrm{Hz}}$) yields the detector's signal transfer function in digital units/strain.

Next, we measure the noise spectra under normal detector operating conditions (in digital units/$\sqrt{\mathrm{Hz}}$) and divide the result by the experimentally determined signal response transfer function. This yields the equivalent input strain noise spectrum in units of strain/$\sqrt{\mathrm{Hz}}$. Near the resonant modes, the strain noise spectrum is limited by transducer force noise. Away from the resonances, it is limited by the SQUID white noise. The strain noise spectrum dips to a local minimum at each of the mode frequencies, indicating that, as expected, the detector is most sensitive at those frequencies. The current sensitivity of ALLEGRO as of 1998 is shown in Fig. 11.

The dip in the strain noise spectrum at frequencies below

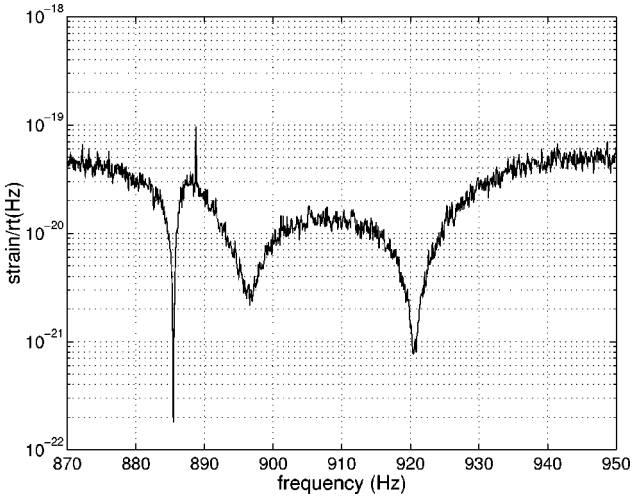

FIG. 11. The equivalent input strain-noise spectrum of the ALLEGRO detector as of 1998.

the extra mode frequency is an artifact of the unwanted force generator resonance and the SQUID white noise. It is not a useful frequency for gravity wave detection. The artifact is understood by noting that Eq. (A28) produces less force at certain frequencies immediately below the extra mode frequency. Although the force applied by the force generator is less than for other frequencies in this region, the output is dominated by the white noise of the SQUID which is insensitive to the magnitude of force applied by the force generator. Our calculated response thus produces a big artificial peak here. In the absence of SQUID white noise, the response here would also be small, and no dip would be observed.

IX. CONCLUSION

In this paper, we describe the three normal mode transfer functions needed to describe a resonant mass gravitational wave antenna. We gain several new insights from this picture. The mistuning between the antenna and transducer can be experimentally determined. The uncoupled frequencies of the antenna and transducer and the effective mass of the transducer can be inferred from measurements of the mistuning. The detector transfer functions which include this mistuning explain why γ_+ does not equal γ_- in either the Stanford or LSU antennas.

We develop a new set of detector diagnostics based on these transfer functions. The measurement of the mixing angle via the driving point response should be consistent with the measurement of the mixing angle via the autocorrelation functions. The amplitude of excitation of the two modes after a short burst should be nearly equal in response to a broadband impulse. Deviations from the ideal behavior can be used to quantify the effects of parasitic resonances near the detection modes. The experimental results demonstrate that the behavior of ALLEGRO is truly that of two coupled, noise-driven oscillators.

This model offers new insight into the conventions used to describe the output of a resonant antenna in terms of an incident excitation. In response to a burst, the total energy deposited into the antenna is not equally divided between the two modes. The partitioning of the energy depends upon the degree of detector mistuning. Conventions derived from the amount of force applied to the antenna describe the relationship between an incident excitation and the output of the readout system without any references to antenna dependent mistuning.

Finally, an analogue of this model is a starting point for understanding how to interpret results from the multimode transducers under development. This model, extended to three modes, will be an important tool in both developing a calibration procedure for and understanding the noise sources of three-mode antennas.

ACKNOWLEDGMENTS

This research was supported by the National Science Foundation under Grant No. PHY-9311731.

APPENDIX: THE COMPLETE ANTENNA-TRANSDUCER-FORCE GENERATOR SOLUTION

Equations (12) and (17) completely describe the dynamics of the coupled antenna-transducer-force generator system. The coupled antenna-transducer is treated as a load connected to the mechanical port of the force generator. To this point, we have ignored effects produced by the coupling of the force generator to the antenna-transducer system. Physically, the coupling of the force generator to the system (even in the absence of a resonance) changes the mode frequencies and amplitudes measured at the readout system. This appendix discusses the deviations from the ideal created by a force generator with non-infinitesimal mass. This calculation is used to determine the magnitude of the perturbation caused by the additional resonance in the force generator.

1. Antenna force-generator interaction

When a calibration signal is applied, the following conditions are true: (1) $\tilde{V}_p$ is constant, fixed by a voltage source. (2) The only external force acting on the bar comes from the force generator, $\tilde{F}_1 = -\tilde{F}_p$. The sign difference arises from the convention that $\tilde{F}_p$ and $i\omega\tilde{x}_p$ are defined so that power flows into the mechanical port of a transducer [21]. (3) The mechanical port of the force generator is rigidly attached to the antenna face, $\tilde{x}_1 = \tilde{x}_p$. (4) There is no external force acting directly on the transducer, $\tilde{F}_2 = 0$. (It is assumed that the effects of Brownian noise at the bar-transducer interface can be neglected). Given these 4 conditions, it is possible to solve Eqs. (12) and (17) together in order to obtain $\tilde{x}_1$ and $\tilde{x}_2$ in terms of $\tilde{V}_p$. The result is

$$\begin{bmatrix} \tilde{x}_1 \\ \tilde{x}_2 \end{bmatrix} = \frac{1}{1 + i\omega \dfrac{\|Z\|}{Z_{22}} G_{11}} \begin{bmatrix} G_{11} & G_{12} \\ G_{21} & G_{22} + i\omega \dfrac{\|Z\|}{Z_{22}} \|G\| \end{bmatrix} \times \begin{bmatrix} -\dfrac{Z_{12}}{Z_{22}} \tilde{V}_p \\ 0 \end{bmatrix}. \tag{A1}$$

$\|Z\|$ is the determinant of the force generator electromechanical impedance matrix.

When the bar is operated as a detector, these conditions are different. In this mode of operation, (1) the ac voltage across the force generator is set to zero, $\tilde{V}_p = 0$; (2) the force applied to the antenna is the sum of any external force on the bar (such as an incident gravity wave) plus any response from the short-circuited force generator, $\tilde{F}_1 = -\tilde{F}_p + \tilde{F}_{ext1}$; (3) there may be some external $\tilde{F}_2 = \tilde{F}_{ext2}$ present. Condition (4), $\tilde{x}_1 = \tilde{x}_p$, remains the same. In this case, in terms of the external forces,

$$\begin{bmatrix} \tilde{x}_1 \\ \tilde{x}_2 \end{bmatrix} = \frac{1}{1 + i\omega \dfrac{\|Z\|}{Z_{22}} G_{11}} \begin{bmatrix} G_{11} & G_{12} \\ G_{21} & G_{22} + i\omega \dfrac{\|Z\|}{Z_{22}} \|G\| \end{bmatrix} \begin{bmatrix} \tilde{F}_{ext1} \\ \tilde{F}_{ext2} \end{bmatrix}. \tag{A2}$$

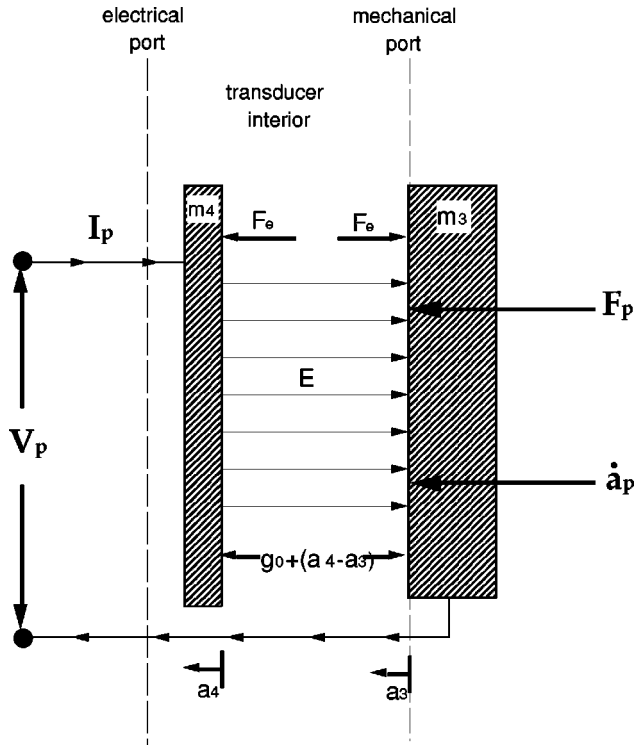

FIG. 12. Schematic of the simplest possible configuration for a capacitive force generator, a parallel plate capacitor whose plates are free to move under the force of the electric field between them.

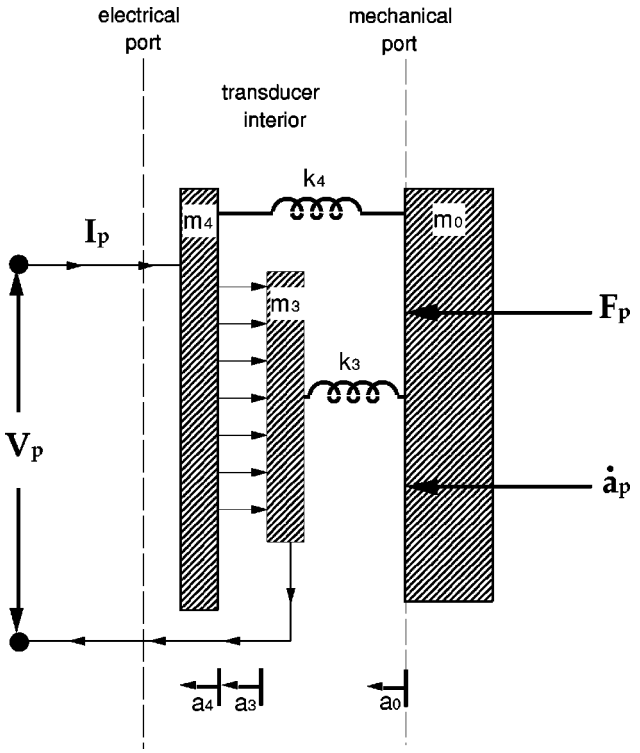

FIG. 13. Schematic of a general electromechanical force generator, which is a system of coupled harmonic oscillators with two of the masses connected by an electric field instead of springs.

From these equations it is clear that the effect of applying a voltage V_p to the force generator described by Eq. (A1) is exactly the same as applying a force of magnitude $\tilde{F}_{ext1} = -(Z_{12}/Z_{22})\tilde{V}_p$ directly to the bar.

Ideally, the force generator has no resonances near the detection modes of the coupled antenna-transducer. In this case, both $\|Z\|/Z_{22}$ and Z_{12}/Z_{22} are approximately constant within the detection bandwidth and the denominator term depending on $\|Z\|/Z_{22}$ primarily contributes a small frequency shift. We recover the relations

$$\tilde{x}_1 \approx G_{11}\tilde{F}_1. \tag{A3}$$

$$\tilde{x}_2 \approx G_{21}\tilde{F}_1. \tag{A4}$$

In the case of resonances, however, we shall have to more carefully consider the effect of these denominators.

2. General electrostatic transducer

The heart of the capacitive force generator (illustrated in Fig. 12) is a parallel plate capacitor whose plates are free to move. The equations relating the voltages and currents inside of the transducer to its internal mechanical dynamics are derived from the equation for force on the plates of a parallel plate capacitor, $F = CE^2\Delta x/2$, and the derivative of the definition of capacitance, $I = C\dot{V} + \dot{C}V$, where F is the force on a single capacitor plate, C is the capacitance of the plates, E is the electric field between the plates, Δx is the separation between the plates, and V and I are the voltage and current across the plates, respectively. The transducer is operated by applying a small ac voltage in addition to a large dc voltage. Under this condition the relationships between $\tilde{F}_e$, the time-varying electrical force on the capacitor plates due to the electric field, $\tilde{V}_{ac}$, the time-varying voltage across the capacitor plates, $\tilde{I}_{ac}$, the time-varying and current across the capacitor plates, and $\tilde{x}_3$ and $\tilde{x}_4$, the inertial coordinates of the two capacitor plates (the conventions that m_1 represents the antenna and m_2 represents the inductive transducer are retained through this appendix), are linear:

$$\tilde{F}_e = C_0E_0\tilde{V}_{ac} - C_0E_0^2(\tilde{x}_4 - \tilde{x}_3), \tag{A5}$$

$$\tilde{V}_{ac} = \frac{\tilde{I}_{ac}}{i\omega C_0} + E_0(\tilde{x}_4 - \tilde{x}_3). \tag{A6}$$

C_0 and E_0 are the size of the capacitance and strength of the electric field when only the dc field is present.

Physically, a capacitive force generator is a set of coupled harmonic oscillators (illustrated in Fig. 13) with two masses connected by an electric field instead of springs. Its mechanical dynamics are described with a Green's function matrix. The electrostatic forces enter the problem as a pair of equal and opposite external forces acting on masses m_3 and m_4. There is also an external force on the mechanical port, $\tilde{F}_0$, resulting from the force generator's interaction with the antenna. For a system composed of N masses,

$$\begin{bmatrix} \tilde{x}_0 \\ \tilde{x}_3 \\ \tilde{x}_4 \\ \cdots \\ \tilde{x}_N \end{bmatrix} = \begin{bmatrix} G_{00} & G_{03} & G_{04} & \cdots & G_{0N} \\ G_{30} & G_{33} & G_{34} & \cdots & G_{3N} \\ G_{40} & G_{43} & G_{44} & \cdots & G_{4N} \\ & & & & \\ G_{N0} & G_{N3} & G_{N4} & \cdots & G_{NN} \end{bmatrix} \begin{bmatrix} \tilde{F}_0 \\ \tilde{F}_e \\ -\tilde{F}_e \\ \cdots \\ 0 \end{bmatrix}. \tag{A7}$$

Equations (A5), (A6), and (A7) completely describe the motion of the force generator resulting from both electrostatic and mechanical forces. In order to form the impedance matrix for this system, the variables describing motion inside of the force generator ($\tilde{F}_e$, $\tilde{x}_3$, and $\tilde{x}_4$) must be eliminated. The force and velocity of the capacitor plates are concisely described in terms of the voltage and current at the electrical port by rewriting Eqs. (A5) and (A6) in their transfer matrix representation,

$$\begin{bmatrix} \tilde{F}_e \\ i\omega\tilde{q} \end{bmatrix} = \begin{bmatrix} 0 & \dfrac{E_0}{i\omega} \\ \dfrac{i\omega}{E_0} & \dfrac{-1}{C_0 E_0} \end{bmatrix} \begin{bmatrix} \tilde{V}_p \\ \tilde{I}_p \end{bmatrix}, \tag{A8}$$

$$q = x_4 - x_3. \tag{A9}$$

Equation (A8) assumes that the voltage and current at the port are connected to the capacitor plates by an ideal short circuit, $V_p = V_{ac}$, $I_p = I_{ac}$. Equation (A7) can also be recast in a transfer matrix form relating the force and velocity of the mechanical port to the force and velocity of the capacitor plates,

$$\begin{bmatrix} \tilde{F}_p \\ i\omega\tilde{x}_p \end{bmatrix} = \frac{1}{\mathcal{G}_2} \begin{bmatrix} \mathcal{G}_1 & \dfrac{-1}{i\omega} \\ i\omega(\mathcal{G}_2^2 - G_{00}\mathcal{G}_1) & G_{00} \end{bmatrix} \begin{bmatrix} \tilde{F}_e \\ i\omega\tilde{q} \end{bmatrix}, \tag{A10}$$

$$\mathcal{G}_1 = G_{43} + G_{34} - G_{44} - G_{33}, \tag{A11}$$

$$\mathcal{G}_2 = G_{30} - G_{40}. \tag{A12}$$

This assumes that m_0 has been defined as the mechanical port of the force generator, so that $\tilde{x}_p = \tilde{x}_0$ and $\tilde{F}_p = -\tilde{F}_0$. The right side of Eq. (A8) is used to eliminate $\tilde{F}_e$ and $\tilde{q}$ from Eq. (A10). Rearranging the result into an impedance matrix form, the general electrostatic impedance matrix is

$$\begin{bmatrix} \tilde{F}_p \\ \tilde{V}_p \end{bmatrix} = \begin{bmatrix} \dfrac{-1}{i\omega G_{00}} & \dfrac{E_0 \mathcal{G}_2}{i\omega G_{00}} \\ \dfrac{E_0 \mathcal{G}_2}{i\omega G_{00}} & \dfrac{1}{i\omega C_0} - \dfrac{E_0^2}{i\omega} \dfrac{(\mathcal{G}_2^2 - \mathcal{G}_1 G_{00})}{G_{00}} \end{bmatrix} \begin{bmatrix} i\omega\tilde{x}_p \\ \tilde{I}_p \end{bmatrix}. \tag{A13}$$

Note that the necessary symmetry property between the off-diagonal elements is present.

3. Calculating the effect of a resonant force generator

Using Eq. (A13), we can determine the frequency dependence of $\|Z\|/Z_{22}$ and $\mathcal{Z}(\omega)$ without relying on detailed knowledge of the force generator geometry. From linear network theory, it is known that the inverse of the driving point response function G_{00} is also a driving point response function. This implies that $1/G_{00}$ can be written as a partial fraction expansion. Since there is only a single additional resonance in ALLEGRO, all but one of the terms of this expansion can be combined into a single, frequency-independent constant. The remaining term is written as a constant coefficient over a resonant denominator.

The first quantity needed is $\|Z\|/Z_{22}$. Since C_0 is small, Z_{22} is nearly constant, $Z_{22} \approx 1/i\omega C_0$. Under this assumption,

$$\frac{\|Z\|}{Z_{22}} = \frac{1}{i\omega}\left(\beta_0 + \frac{\beta_1}{(\omega^2 - \omega_X'^2)}\right), \tag{A14}$$

where ω_X' is the frequency of the extra resonance in the force generator. The form of the generator constant in the resonant case is also a partial fraction expansion with a single frequency-dependent term of interest,

$$\frac{Z_{12}}{Z_{22}} = \beta_2 + \frac{\beta_3}{(\omega^2 - \omega_X'^2)}. \tag{A15}$$

All of the β's are real-valued constants. There is no obvious relationship between the different β's in this representation. The denominator frequency is the same in both expressions.

Substituting Eqs. (A14) and (A15) into Eq. (A1), the driving point response of the system becomes

$$\frac{G_{11}}{\Delta}\left(\frac{-Z_{12}}{Z_{22}}\right) = \frac{[\beta_2(\omega^2 - \omega_X'^2) + \beta_3][\cos^2\theta(\omega_-'^2 - \omega^2) + \sin^2\theta(\omega_+'^2 - \omega^2)]}{m_1(\omega_-'^2 - \omega^2)(\omega_+'^2 - \omega^2)(\omega^2 - \omega_X'^2) + [\beta_0(\omega^2 - \omega_X'^2) + \beta_1][\cos^2\theta(\omega_-'^2 - \omega^2) + \sin^2\theta(\omega_+'^2 - \omega^2)]}, \tag{A16}$$

where $\Delta = 1 + i\omega\|Z\|G_{11}/Z_{22}$ to make the notation more compact. The primed frequencies ω_+' and ω_-' are the result of coupling the bare bar to the transducer. They are not observable once the system is assembled. The unprimed frequencies ω_+ and ω_- are the result of coupling the antenna, transducer, and force generator together,

$$\omega_\pm' = \omega_\pm + \delta_\pm. \tag{A17}$$

$\delta_\pm$ is the frequency shift of the normal modes of the detector created when the force generator is added to the system. Though this additional frequency shift is physically uninteresting, the unprimed frequencies are known with great accuracy and are

most useful for comparison between model and experiment. Experimentally it is known that these frequency shifts are small. There is an analogous frequency shift of ω_X' to a value ω_X when the force generator is coupled to the bar.

Consider first the measurement of $\gamma_\pm$. In this case, substituting Eq. (A17) into Eq. (A16), yields a driving point transfer function of

$$\frac{G_{11}}{\Delta}\left(\frac{-Z_{12}}{Z_{22}}\right)=\frac{[\beta_2(\omega^2-\omega_X^2-2\delta_X\omega_X)+\beta_3][\cos^2\theta(\omega_-^2+2\delta_-\omega_--\omega^2)+\sin^2\theta(\omega_+^2+2\delta_+\omega_+-\omega^2)]}{m_1(\omega^2-\omega_X^2)(\omega_-^2-\omega^2)(\omega_+^2-\omega^2)}. \tag{A18}$$

Mathematically, including the correction term in the denominator changes the positions of the poles of the transfer functions without changing the position of the zeros. The time-domain amplitude of $x_1(t)$ takes the form of Eqs. (25) and (26) plus a correction term due to the additional residue at ω_X. The value of $\gamma_\pm$ is thus proportional to the product of the frequency dependent Z_{21}/Z_{22} and the amplitude of $x_1(t)$:

$$\gamma_+=\frac{(\cos^2\theta+\epsilon_1)}{m_1}\left(\beta_2(1-\epsilon_{3+})+\frac{\beta_3}{(\omega_+^2-\omega_X^2)}\right)^2(1+\epsilon_{3+}), \tag{A19}$$

$$\gamma_-=\frac{(\sin^2\theta-\epsilon_1)}{m_1}\left(\beta_2(1-\epsilon_{3-})+\frac{\beta_3}{(\omega_-^2-\omega_X^2)}\right)^2(1+\epsilon_{3-}), \tag{A20}$$

$$\epsilon_1=\frac{\delta_+\omega_+\sin^2\theta+\delta_-\omega_-\cos^2\theta}{\omega_+^2-\omega_-^2}, \tag{A21}$$

$$\epsilon_{3\pm}=\frac{2\delta_X\omega_X}{\omega_\pm^2-\omega_X^2}. \tag{A22}$$

We can also evaluate the gamma value for the extra mode,

$$\gamma_X=\frac{[\cos^2\theta(\omega_-^2-\omega_X^2)+\sin^2\theta(\omega_+^2-\omega_X^2)+\epsilon_1(\omega_+^2-\omega_-^2)](\beta_3-2\beta_2\delta_X\omega_X)^2}{2m_1\delta_X\omega_X(\omega_+^2-\omega_X^2)(\omega_-^2-\omega_X^2)}. \tag{A23}$$

Using a set of masses and spring constants that approximately describe the force generator mounted on ALLEGRO, these frequency shifts are estimated to be less than 1 Hz. This implies a maximum correction of $\epsilon_1\approx.02$. By comparing the measured ratios of $\gamma_X/\gamma_\pm$ to values predicted by Eqs. (A19)–(A23), we determine that $\delta_X<0.1$ Hz, and $\epsilon_{3\pm}<0.01$.

In the case of the mode amplitudes measured after an excitation of the bar, the frequency shifts change the force-generator-voltage–transducer-motion transfer function to

$$\frac{G_{21}}{\Delta}\left(\frac{-Z_{12}}{Z_{22}}\right)=\frac{\sin\theta\cos\theta[\beta_2(\omega^2-\omega_X^2-2\delta_X\omega_X)+\beta_3][\omega_+^2-\omega_-^2+2(\delta_+\omega_+-\delta_-\omega_-)]}{\sqrt{m_1m_2}(\omega^2-\omega_X^2)(\omega_-^2-\omega^2)(\omega_+^2-\omega^2)}. \tag{A24}$$

Assuming frequency shifts of approximately 1 Hz, ϵ_2 will be on the order of 5×10^{-4}. The measured post-excitation mode amplitudes are directly proportional to the residues of Eq. (A24) evaluated at ω_+ and ω_-,

$$P_+\propto\frac{-\sin\theta\cos\theta}{\sqrt{m_1m_2}\omega_+}\left(\beta_2(1-\epsilon_{3+})+\frac{\beta_3}{(\omega_+^2-\omega_X^2)}\right)(1+\epsilon_2), \tag{A25}$$

$$P_-\propto\frac{\sin\theta\cos\theta}{\sqrt{m_1m_2}\omega_-}\left(\beta_2(1-\epsilon_{3-})+\frac{\beta_3}{(\omega_-^2-\omega_X^2)}\right)(1+\epsilon_2), \tag{A26}$$

$$\epsilon_2=\frac{2(\delta_+\omega_+-\delta_-\omega_-)}{\omega_+^2-\omega_-^2}. \tag{A27}$$

The important result of this formalism is that the mixing angle is still the only parameter needed to characterize the mistuning between the antenna and transducer, but the voltage-to-force relationship is no longer described by a constant. Neglecting the small corrections (less than 1%) caused by the $(1+\epsilon_{3\pm})$ terms in Eqs. (A19) and (A20), we absorb all of the perturbation created by the extra mode into the voltage-to-force constant. In the notation of the previous sections, $\mathcal{Z}(\omega)$ is now a function of frequency,

$$\mathcal{Z}(\omega_{\pm}) = \beta_2(1-\epsilon_{3\pm}) + \frac{\beta_3}{(\omega_{\pm}^2 - \omega_X^2)}. \tag{A28}$$

Using Eq. (A28), Eqs. (A19) and (A20) become Eqs. (43) and (44), and Eqs. (A25) and (A26) become Eqs. (45) and (46).

[1] P. Astone *et al.*, Phys. Rev. D **47**, 362 (1993).
[2] M. Cerdonio *et al.*, in *Gravitational Wave Experiments*, edited by E. Coccia *et al.* (World Scientific, New York, 1995).
[3] D. G. Blair *et al.*, Phys. Rev. Lett. **74**, 1908 (1995).
[4] E. Mauceli *et al.*, Phys. Rev. D **54**, 1264 (1996).
[5] K. S. Thorne, in *300 Years of Gravitation*, edited by S. W. Hawking and W. Israel (Cambridge University Press, Cambridge, England, 1987).
[6] G. W. Gibbons and S. W. Hawking, Phys. Rev. D **4**, 2191 (1971).
[7] R. Giffard, Phys. Rev. D **14**, 2478 (1976).
[8] Ho Jung Paik, Ph.D. thesis, Stanford University, 1974.
[9] P. F. Michelson and R. C. Taber, J. Appl. Phys. **52**, 4313 (1981).
[10] Jean-Paul Richard, Phys. Rev. Lett. **52**, 165 (1984).
[11] John C. Price, Phys. Rev. D **36**, 3555 (1987).
[12] N. Solomonson *et al.*, Phys. Rev. D **46**, 2299 (1992).
[13] Bu-Xin Xu *et al.*, Phys. Rev. D **40**, 1741 (1989).
[14] S. Boughn *et al.*, Rev. Sci. Instrum. **61**, 1 (1990).
[15] Charles W. Misner, Kip S. Thorne, and John Archibald Wheeler, *Gravitation* (Freeman, New York, 1973).
[16] L. D Landau and E. M. Lifshitz, *Theory of Elasticity*, 3rd ed. (Pergamon, New York, 1986).
[17] K. Tsubono, in *The Detection of Gravitational Waves*, edited by D. Blair (Cambridge University Press, New York, 1991).
[18] James Randolph Marsden, Ph.D. thesis, University of Rochester, 1984.
[19] N. Solomonson *et al.*, Rev. Sci. Instrum. **65**, 174 (1994).
[20] Louis A. Pipes, *Matrix Methods for Engineering* (Prentice-Hall, Engelwood Cliffs, NJ, 1963), Chap. 8.
[21] H. K. P. Neubert, *Instrument Transducers* (Oxford University Press, Oxford, 1975).
[22] Robert N. McDonough and Anthony D. Whalen, *Detection of Signals in Noise* (Academic, New York, 1995).
[23] A. Papoulis, *Probability, Random Variables and Stochastic Processes* (McGraw-Hill, New York, 1965).